Inorganic Chemistry

Article

pubs.acs.org/IC

Speciation of Ferric Phenoxide Intermediates during the Reduction of Iron(III)−μ-Oxo Dimers by Hydroquinone

William D. Kerber,*[,†] Kaitlyn A. Perez,[†] Chuqiao Ren,[†] and Maxime A. Siegler[‡]

[†]Department of Chemistry, Bucknell University, Lewisburg, Pennsylvania 17837, United States

[‡]Department of Chemistry, Johns Hopkins University, Baltimore, Maryland 21218, United States

Supporting Information

ABSTRACT: The aqueous speciation of iron(III)−tris-(pyridylmethyl)amine (TPA) complexes was determined from potentiometric titration data, and the overall formation constants (β) for relevant species were calculated. At pH < 3 the mononuclear complex $[Fe(TPA)]^{+3}(aq)$ predominates (log β = 10.75(15). Above pH 3 $Fe^{3+}-OH_2$ hydrolysis produces the μ-oxo dimer $[Fe_2(\mu\text{-}O)(TPA)_2(H_2O)_2]^{+4}$ (**1a**; log β = 19.91(12)). This species is a diprotic acid with the conjugate bases $[Fe_2(\mu\text{-}O)(TPA)_2(H_2O)(OH)]^{+3}$ (**1b**; log β = 15.53(6)) and $[Fe_2(\mu\text{-}O)(TPA)_2(OH)_2]^{+2}$ (**1c**; log β = 10.27(7)). The pK_as of **1a** are 4.38(14) and 5.26(9). Compounds **1a−c** quantitatively oxidize hydroquinone to benzoquinone with concomitant formation of 2 equiv of Fe(II). Kinetic and spectroscopic data at pH 5.6 are consistent with rapid equilibrium formation of a diiron(III)−phenoxide intermediate followed by rate-controlling electron transfer. The equilibrium constant for the formation of the intermediate complex is 25(3) M^{-1}, and the rate constant for its decomposition is 0.56(9) s^{-1}. A kinetic isotope effect of k_H/k_D = 1.5 was determined from proton inventory experiments in mixed H/D media. The μ-oxo−diiron(III) phenoxide intermediate is hydrolyzed in a pH dependent process to form a mononuclear iron(III)−phenoxide, which complicates the kinetics by introducing a fractional dependence on total iron(III) concentration in the pH range 4.1−5.2. The pH-dependent cleavage of μ-oxo−diiron(III)−phenoxides was investigated with phenol, a redox-inert proxy for hydroquinone. The addition of phenol to **1** facilitates acidic cleavage of the μ-oxo dimer to form $[Fe(TPA)(OPh)(H_2O)]^{+2}$, which becomes the dominant iron(III)−phenoxide as the pH decreases to 4. The 2-naphtholate analogue of this intermediate, $[Fe(TPA)(2\text{-naphtholate})(OCH_3)]ClO_4$ (**6**), was characterized by single-crystal X-ray diffraction ($C_{29}H_{28}FeN_4O_2ClO_4$; $P2_1$; a = 13.2646(2) Å, b = 15.2234(3) Å, c = 13.7942(3) Å; Z = 4).

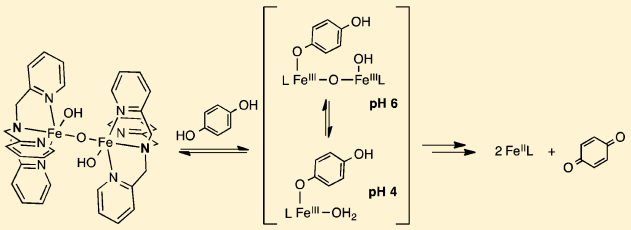

INTRODUCTION

Iron(III) has a rich and varied aqueous coordination chemistry because it has a flexible geometry and coordination number, it undergoes facile ligand substitution, and it is a hard Lewis acid that enhances the Brønsted acidity of coordinated water molecules. The later promotes hydrolysis and formation of multinuclear complexes based on the Fe−O−Fe unit, and the kinetic product of this process is an amorphous orange polymer that crystallizes into various iron oxide phases including ferrihydrite, goethite, and hematite.[1] All of these materials are relatively insoluble at neutral pH (−log K_{sp} = 36−42). The concentration of dissolved iron(III) in natural waters is frequently not as low as predicted by mineral solubility alone, especially if there is also organic material present. The ferric ion is strongly complexed by natural organic ligands that arrest hydrolysis and precipitation and stabilize mono- and multinuclear iron complexes in the water column.[2]

Biological systems exploit the stability of the $Fe^{3+}-O-Fe^{3+}$ unit in metalloenzymes with multiple bridged iron atoms that work cooperatively to accomplish difficult redox transformations.[3] This strategy is exemplified by non-heme diiron enzymes such as hemerythrin (Hr), soluble methane monooxygenase (sMMO), and ribonucleotide reductase (RNR), which are used by a variety of organisms for selective O_2 binding/activation.[4] These systems have inspired chemists to devise synthetic strategies for controlled iron(III) hydrolysis to study the novel chemical and magnetic properties of these materials. A wide range of ligand architectures have been explored; one notable example is tris(pyridylmethyl)amine (TPA), a tripodal ligand that has been used to prepare a range of dinuclear iron complexes based on the Fe−O−Fe unit. Previous investigations have successfully mapped out the redox chemistry and structural interconversions of diiron complexes as models of non-heme diiron metalloenzymes. A variety of dibridged $Fe^{III}{}_2(\mu\text{-}O)(\mu\text{-}X)(TPA)_2$ complexes have been prepared where X is an anionic oxygen donor.[5] Electron-rich TPA derivatives stabilize the $Fe_2(\mu\text{-}O)_2$ "diamond core" in a variety of oxidation states ($Fe_2^{III,III}$, $Fe_2^{III,IV}$, $Fe_2^{IV,IV}$);[6,7] the diferryl complex is a model of the elusive intermediate Q in sMMO.

In the presence of water, the $Fe_2(\mu\text{-}O)_2$ diamond core is in equilibrium with the hydrated form (HO)Fe(μ-O)Fe(OH), with the latter structure favored for the unsubstituted TPA

Received: June 17, 2014
Published: October 16, 2014

   dx.doi.org/10.1021/ic5014347 | *Inorg. Chem.* 2014, 53, 11507−11516

Chart 1. Diiron(III)−TPA Complexes with a Single Bridging Ligand[a]

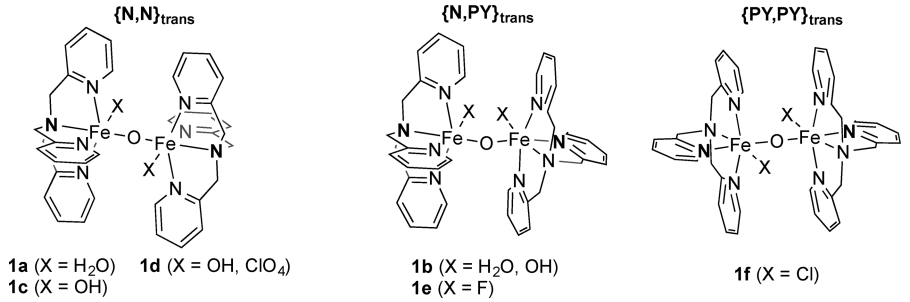

[a]Each TPA ligand may adopt one of two isomeric forms (N_{trans} or PY_{trans}). See ref 8.

ligand. $Fe_2(\mu\text{-}O)(X)_2(TPA)$ complexes that have been characterized crystallographically are shown in Chart 1.[8] Note that three isomeric structures are possible for each complex depending on the identity of the donor atom *trans* to the oxo bridge. Reactivity studies on diiron(III)−TPA complexes have generally focused on accessing high-valent states ($Fe_2^{III,IV}$ or $Fe_2^{IV,IV}$) that mimic reactive species like sMMO intermediate Q, although reduction to the diferrous state is also an important part of the catalytic cycle for O_2 activation. Enzymatically this is accomplished by electron transfer from an oxidoreductase to iron(III), but μ-oxo dimers may also be reduced by a variety of chemical means including hydroquinones,[9a] ascorbic acid,[9b,c] cyclohexadiene,[9d] hydrazines,[9e,f] pyruvic acid,[9g] and nitrite.[9h]

Although the tris(pyridylmethyl)amine ligand has proven itself extremely valuable for the investigation of μ-oxo diiron coordination chemistry, the thermodynamics of the aqueous iron(III)−TPA system have not been investigated. We report here the pH-dependent speciation of iron(III)−TPA complexes as well as their reactivity with 1,4-dihydroxybenzene (hydroquinone). Phenols are a biologically important class of ligands for iron and create a unique chromophore at 400−600 nm ascribed to phenolate-to-iron(III) LMCT (LMCT = ligand-to-metal charge transfer). A variety of metalloenzymes have this feature due to the presence of a tyrosine side chain in the active site. Examples include transferrins, purple acid phosphatases (so-named for the characteristic LMCT band), and catechol dioxygenases.[10] The latter have been modeled with iron(III)−TPA complexes such as $[Fe(TPA)(catecholate)]^+$,[11] which is structurally similar to the intermediates found during the reaction of **1** with hydroquinone, *vide infra*. Iron(III)−TPA−hydroquinone complexes have a pH-dependent speciation: mononuclear complexes are favored under acidic conditions while μ-oxo dimers are found at circumneutral pH. Unlike $[Fe(TPA)(catecholate)]^+$, iron(III)−TPA−hydroquinone complexes are not thermally stable and decompose rapidly at 25 °C to give iron(II) and benzoquinone (BQ).

EXPERIMENTAL SECTION

General Considerations. Aqueous iron(III)−TPA complexes were prepared *in situ* and equilibrated prior to use. All reagent solutions were prepared in a COY Laboratories anaerobic chamber containing <1 ppm of O_2. The atmosphere was additionally scrubbed with soda lime, to remove CO_2, and activated charcoal, to remove trace organic vapors. Hydroquinone, benzoquinone, and 2-naphthol were purchased from Aldrich and sublimed under vacuum. TPA was purchased from TCI and stored under N_2. Acetonitrile and methanol were spectrophotometric grade and were used without additional purification. All other reagents were purchased from Aldrich or Acros and used as received.

Reagent Solutions. All reagents were prepared as concentrated stock solutions in ultrapure water (18 MΩ·cm^{-1}; glass distilled under N_2) and stored in brown glass bottles under N_2, except NaOH, which was stored in plastic under N_2. TPA(aq) was solubilized by addition of HNO_3. $Fe(NO_3)_3$(aq) was standardized by titration with Na_2EDTA to the variamine blue end point[12] (Na_2EDTA = disodium ethylenediaminetetraacetic acid). Na_2EDTA was standardized by titration against $CaCO_3$ to the Eriochrome black T end point. Carbonate-free sodium hydroxide was prepared by dissolving solid NaOH in an equal mass of water and allowing the insoluble Na_2CO_3 to settle out of solution.[12] The supernatant was removed, diluted to approximately 0.1 N, and standardized against potassium hydrogen phthalate to the potentiometric end point. Commercial 0.1 N HNO_3 was standardized against sodium tetraborate to the potentiometric end point.

Titration Apparatus. Titrations were performed using a Metrohm Titrando 888 automatic titrator equipped with a Metrohm Unitrode pH electrode (1.00 M KNO_3 reference electrolyte). The titrator was equipped with a 20 mL buret with an accuracy of ±0.03 mL for reagent standardization and a 1 mL buret with an accuracy of ±0.003 mL for stability constant determination. Temperature was controlled when necessary with a jacketed titration vessel and a recirculating water bath. Air was excluded when necessary by purging with a stream of prehumidified N_2(g).

Stability Constant Determination. Glass electrode calibration was performed twice daily, once before and once after any iron(III)−TPA titrations. The GLEE method[13] was used to determine the electrode standard potential and slope, and the average daily values were used to convert raw mV readings to pH. A junction potential correction factor was applied to electrode calibrations using the VLpH method[14] when titrations were performed below pH 2.5.

A Typical Titration Procedure Is As Follows. To a titration vessel in an anaerobic chamber was added 427.0 mg of $NaNO_3$ (5.024 mmol) dissolved in 50.00 mL of water, 0.100 mL of a 0.1002 M solution of $Fe(NO_3)_3$ (10.02 μmol), 0.750 mL of a 0.0400 M TPA solution also containing 0.0198 M HNO_3 (30.0 μmol of TPA; 14.8 μmol of HNO_3), and 0.140 mL of a 0.1043 M solution of NaOH (14.6 μmol). Air was excluded during the titration, and the temperature was maintained at 25.0 ± 0.1 °C. The initial pH was 5.420 and the initial ionic strength 0.100 M. After 30 min no precipitated FeOOH(s) was observed, and the solution was titrated to pH 2.111 using 0.1001 N HNO_3. Aliquot size was 0.010 mL up to 0.4 mL of titrant (pH 3.6) and then 0.077 mL up to 5 mL of total titrant. The delay time between aliquots was 180 s to provide adequate time for the system to re-establish equilibrium.

Stability constants (log β) were determined by fitting the proposed speciation model to titration data using the nonlinear least-squares routine in the software Hyperquad2008.[15] Titration curves were fit individually, and the results are shown in Table S2 in the Supporting Information. The final log β values in Table 1 are reported as averages. TPA protonation constants were determined separately (Table S3 in the Supporting Information), and Fe^{3+}(aq) hydrolysis constants were taken from the literature.[16] The latter two were held constant when refining iron(III)−TPA stability constants. A minimum of 20 ⟨mV, mL⟩ data points were collected per refined stability constant in a given

dx.doi.org/10.1021/ic5014347 | *Inorg. Chem.* 2014, 53, 11507−11516

titration. Log K_w was taken to be −13.78 (25 °C; I = 0.100 M). Speciation diagrams were created using the software Hyss2009.[17] See Supporting Information for a more detailed discussion of stability constant determination.

Spectrophotometric Titrations. The general procedure for potentiometric titrations was adapted by adding an Ocean Optics TP300 transmission dip probe to the titration vessel. The probe tip was adjusted to give a path length of 10−20 mm depending on the concentration and intensity of the relevant chromophore. The entire apparatus was protected from ambient light. The probe was interfaced with an Ocean Optics USB2000+ spectrophotometer and a DT-mini-2-GS light source. The spectrometer was triggered by TTL pulse from the autotitrator such that one spectrum was recorded per ⟨mV, mL⟩ data point.

Reaction Kinetics. Kinetic experiments were performed by mixing equal volumes of an iron(III)−TPA solution with a hydroquinone solution in an Applied Photophysics RX-2000 two-channel stopped-flow mixer interfaced with an Ocean Optics USB4000 spectrophotometer (HL-2000 halogen light source). The reactions were performed under N_2 at 25.0 ± 0.1 °C and I = 0.100 M. The integrated absorbance from 480 to 510 nm was monitored at 15−150 ms intervals. A minimum of four replicate trials were performed for each experiment. Iron(III)−TPA solutions were equilibrated for about 30 min prior to reaction. Spectrophotometric titration experiments indicate that iron(III)−TPA complexes reach equilibrium in <1 min in aqueous solution.

A typical kinetics experiment is as follows: an iron(III)−TPA mixture was prepared from stock solutions in an anaerobic chamber at 2× the desired concentration: 1.98 mM in $Fe(NO_3)_3$ and 20.0 mM in TPA with 11.9 mM total HNO_3 and 88.1 mM $NaNO_3$. The amount of HNO_3 necessary to achieve the desired pH was estimated from the speciation model using Hyss2009; the actual pH was measured to be 5.56 after 1:1 dilution with an 88.1 mM $NaNO_3$ solution. The initial ionic strength was calculated to be 0.100 M. A hydroquinone solution was also prepared at 2× the desired concentration: 160 mM hydroquinone and 88.1 mM $NaNO_3$. The two solutions were loaded into gastight syringes with 3-way luer valves and transferred to the stopped-flow mixer under N_2 at 25 °C. Spectra were collected at 38 ms intervals after mixing the two solutions in a 1:1 ratio.

Observed first order rate constants were obtained from exponential fits of absorbance vs time data using the software SigmaPlot. Data were collected for a minimum of 10 half-lives, and good first order behavior was confirmed from log plots. The 10-fold excess of TPA in the reaction ensured against FeOOH(s) precipitation and provided a pH buffer. The pH of the spent reaction solution was measured, and in all cases ΔpH was less than 0.1 unit.

Kinetic Isotope Effects. Rate constants in mixed isotopic media were measured as described above except that H_2O was partially replaced with D_2O. The deuterium mole fraction (n) was calculated from the entire pool of acidic hydrogen atoms: water, nitric acid, and hydroquinone. The two reactant solutions for a given experiment were prepared at the same n and equilibrated for 24 h prior to use. pL (L = H/D) was calculated from the equation pL = pH + $0.0766n^2$ + $0.3314n$, where pH is the meter reading calibrated for H.[18]

Product Analysis. The reaction of **1** with hydroquinone was performed under the same conditions as kinetics experiments, except that [TPA] was decreased to 4 mM to prevent it from obscuring benzoquinone in the HPLC chromatogram, *vide infra* (HPLC = high performance liquid chromatography). Four milliliters of an iron(III)−TPA solution was prepared from stock solutions at 1.5× the desired concentration: 1.50 mM in $Fe(NO_3)_3$ and 6.05 mM in TPA with 6.00 mM total HNO_3 and 135 mM $NaNO_3$. The reaction was initiated by adding 2.000 mL of a 0.2005 M hydroquinone solution and stirred for 60 min under N_2 in the dark. The reaction pH was determined to be 4.02 from an identical iron(III)−TPA solution mixed with 2 mL of water.

Benzoquinone was quantified by HPLC using 4-nitrophenol as an internal standard on a Hewlett-Packard 1090 liquid chromatograph with a diode array detector ($\sum Abs_{254,275,300nm}$). The product mixture was separated on a 150 × 4.60 mm Phenomenex Synergi 4 μm Polar-RP column with an isocratic 87:10:3 water−methanol−acetic acid mobile phase at 1 mL/min and 40 °C. A 1 mL aliquot of the reaction solution was mixed with 0.050 mL of a 20.04 mM 4-nitrophenol solution and 0.115 mL of a 30% solution of acetic acid in methanol. Samples were prepared under N_2 and protected from light prior to analysis. The sample was analyzed in triplicate, and the amount of benzoquinone in the reaction was determined from a calibration curve made from authentic samples. Control experiments demonstrated that benzoquinone was stable under the reaction and HPLC analysis conditions.[19]

Ferrous iron was quantified on a HACH DR-2000 spectrometer using procedure 8146, a proprietary version of the 1,10-phenanthroline method.[12] A 1 mL aliquot of the reaction solution was diluted in a 25 mL volumetric flask with the contents of a HACH ferrous iron reagent powder pillow. A blank was prepared by diluting a second reaction aliquot 25:1 in water. Samples were prepared under N_2 prior to analysis. Ferrous iron was determined at 510 nm using the preprogrammed calibration curve. The accuracy of the method was confirmed using authentic samples of ferrous ammonium sulfate.

*Crystal Structure of [Fe(TPA)(2-naphtholate)(OCH$_3$)]ClO$_4$ (**6**).* ***Caution!*** *Perchlorate salts of organic cations are potentially explosive.*[20] *Although no problems were encountered in this work, these materials should be handled carefully and on a small scale.* To a solution of 86.3 mg of $Fe(ClO_4)_3{\cdot}6H_2O$ (0.187 mmol) and 54.5 mg of TPA (0.188 mmol) in 18.7 mL of methanol were added 27.5 mg of 2-naphthol (0.191 mmol) and 78 μL of triethylamine (0.56 mmol). Crystals suitable for X-ray structure determination were grown from this solution after standing at 5 °C for 1 week. The compound was isolated by filtration, washed with cold methanol, and dried under vacuum to yield 2.5 mg (2.2%) of dark red crystals; ε_{540nm} = 1800 M^{-1} cm^{-1} (CH_2Cl_2).

Data collection and structure refinements were conducted at the Small Molecule X-ray Crystallography Facility at Johns Hopkins University, Baltimore, MD. All reflection intensities were measured at 110(2) K using a SuperNova diffractometer (equipped with Atlas detector) with Cu Kα radiation (λ = 1.54178 Å) under the program CrysAlisPro (Version 1.171.37.33 Agilent Technologies, 2014). The program CrysAlisPro was used to refine the cell dimensions and for data reduction. The structure was solved with the program SHELXS-2013 and was refined on F^2 with SHELXL-2013. Analytical numeric absorption corrections based on a multifaceted crystal model were applied using CrysAlisPro. The temperature of the data collection was controlled using the system Cryojet (manufactured by Oxford Instruments). The H atoms were placed at calculated positions using the instructions AFIX 23, AFIX 43, or AFIX 137 with isotropic displacement parameters having values 1.2 or 1.5 times U_{eq} of the attached C atoms.

The asymmetric unit contains two crystallographically independent formula units (Z' = 2), and the structure is partially disordered. The 2-naphtholate anion coordinated to Fe2 and the two crystallographically independent ClO_4^- counterions are found to be disordered over two orientations, and the occupancy factors of the major components of the disorder refine to 0.568(14), 0.640(11), and 0.589(12), respectively. The absolute structure configuration was established by anomalous-dispersion effects in diffraction measurements on the crystal. The Flack and Hooft parameters refine to −0.004(4) and −0.012(1), respectively.

RESULTS AND DISCUSSION

Iron(III)−TPA Speciation. Aqueous equilibrium constants for iron(III)−TPA complexes were calculated by nonlinear least-squares fitting of potentiometric titration data to a carefully selected speciation model. The results of these experiments are summarized in Table 1. Formation constants (β) are defined as the overall equilibrium of formation of the complex from its component parts (eqs 1−4). The nomenclature β_{abc} refers to the number of (a) iron atoms, (b) TPA molecules, and (c) protons; negative values indicate

dx.doi.org/10.1021/ic5014347 | Inorg. Chem. 2014, 53, 11507−11516

Table 1. Equilibrium Constants for Iron(III)−TPA Complexes

equation	equilibrium constant	
1	log β_{110}	10.75(15)[a]
2	log β_{22-2}	19.91(12)[b]
3	log β_{22-3}	15.53(6)[b]
4	log β_{22-4}	10.27(7)[b]
5	log K_0	−1.6(2)
6	pK_{a1}	4.38(14)
7	pK_{a2}	5.26(9)

[a]Uncertainty given as standard deviation. [b]Uncertainty given as standard error of the mean.

loss of H^+ from coordinated H_2O. The stepwise equilibria in eqs 5−7 were calculated from the overall formation constants.

$$Fe^{+3}(aq) + TPA \overset{\beta_{110}}{\rightleftharpoons} [Fe(TPA)]^{+3}(aq) \quad (1)$$

$$2Fe^{+3}(aq) + 2TPA + 3H_2O \overset{\beta_{22-2}}{\rightleftharpoons} \mathbf{1a} + 2H^+(aq) \quad (2)$$

$$2Fe^{+3}(aq) + 2TPA + 3H_2O \overset{\beta_{22-3}}{\rightleftharpoons} \mathbf{1b} + 3H^+(aq) \quad (3)$$

$$2Fe^{+3}(aq) + 2TPA + 3H_2O \overset{\beta_{22-4}}{\rightleftharpoons} \mathbf{1c} + 4H^+(aq) \quad (4)$$

$$2[Fe(TPA)]^{+3}(aq) \overset{K_0}{\rightleftharpoons} \mathbf{1a} + 2H^+(aq) \quad (5)$$

$$\mathbf{1a} \overset{K_{a1}}{\rightleftharpoons} \mathbf{1b} + H^+(aq) \quad (6)$$

$$\mathbf{1b} \overset{K_{a2}}{\rightleftharpoons} \mathbf{1c} + H^+(aq) \quad (7)$$

The data from Table 1, along with TPA protonation constants and $Fe^{3+}(aq)$ hydrolysis constants (Table S1 in the Supporting Information), were used to generate the pH-dependent speciation diagram shown in Figure 1. At low pH

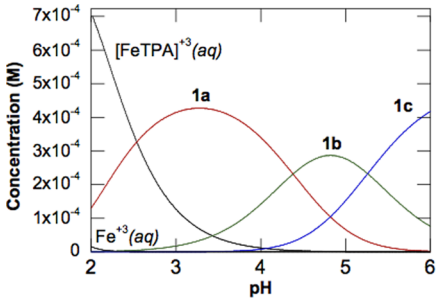

Figure 1. pH-dependent speciation of iron(III)−TPA complexes. Conditions: 0.99 mM Fe^{3+}; 10.0 mM TPA, 25 °C, I = 0.100 M.

Fe^{3+} is strongly complexed by TPA to form the mononuclear species $[Fe(TPA)]^{+3}(aq)$ with log β_{110} = 10.75. This value is consistent with iron(III) binding constants of other polypyridyl ligands.[21] Although $[Fe(TPA)]^{+3}(aq)$ has not been structurally characterized, a κ^4-TPA ligand with at least one coordinated water molecule is expected. Inclusion of formation constant β_{11-1} for the conjugate base $[Fe(TPA)(OH)]^{+2}(aq)$ in the speciation model was not required for successful refinement of the titration data, which indicates that it represents at most a small percentage of the total iron pool. The amount may be estimated as follows: the pK_a of $[Fe(H_2O)_6]^{+3}$ is approximately 2.5,[22] and substitution of water by neutral N donors decreases the acidity by 1−2 log units (See Table S4 in the Supporting Information). This provides a pK_a range of 3.5−4.5 for $[Fe(TPA)]^{+3}(aq)$ and a corresponding log β_{11-1} range of 6.3−7.3. Adding β_{11-1} to the speciation model gives a maximum $[Fe(TPA)(OH)]^{+2}(aq)$ concentration at pH 3.3 that is calculated to be 0.5−5% of the total iron pool at $[Fe^{III}]$ = 1 mM and [TPA] = 10 mM. The amount of $[Fe(TPA)(OH)]^{+2}$ declines rapidly as the pH is raised (less than 0.04% at pH 4.1) due to the favorable dimerization of the Fe^{3+}−OH moiety to form μ-oxo diiron(III) complexes.[23]

The disappearance of mononuclear complexes and concomitant formation of iron(III)−μ-oxo dimers above pH 3 is supported by numerous crystal structures of iron(III)−TPA complexes[8] and by the spectroscopic detection of compound **1** in acetonitrile solution.[8b,d] The two remaining coordination sites at iron are occupied by water, and the pK_a of $[L(H_2O)Fe-O-Fe(OH_2)L]^{+n}$ tracks with the overall positive charge n; **1a** is a tetracation due to the presence of neutral TPA capping ligands, and hence it is relatively acidic with p$K_{a1,2}$ = 4.38 and 5.26. The structurally related complex $[Fe_2(\mu\text{-}O)(phen)_4(H_2O)_2]^{+4}$ exhibits similar pK_a values of 3.71 and 5.28[9e] (phen = 1,10-phenanthroline). Anionic ligands further decrease the acidity of the Fe^{3+}−OH_2 unit as evidenced by the dicationic complexes $[Fe_2(BBPPNOL)(\mu\text{-}OAc)(H_2O)_2]^{+2}$ (p$K_{a1,2}$ = 4.88, 6.33) and $[Fe_2(BPClNOL)_2(H_2O)_2]^{+2}$ (p$K_{a1,2}$ = 5.0, 7.0)[24] (H_3BBPPNOL = *N*,*N*′-bis(2-pyridylmethyl)-*N*,*N*′-bis(2-hydroxybenzyl)-1,3-diaminopropan-2-ol; H_4BPClNOL = [*N*-2-hydroxybenzyl)-*N*-(pyridylmethyl)(3-chloro)(2-hydroxy)]propylamine]). A more extensive list of iron(III)−aquo acidity constants may be found in Table S4 in the Supporting Information.

Structures of Diiron(III)−TPA Complexes. The TPA ligand may occupy two isomeric positions around the Fe−O−Fe unit (N_{Trans} and PY_{Trans} in Chart 1), but the formation constants in Table 1 provide no information about microscopic structure. Simple orbital arguments predict the stability of the diiron(III)−μ-oxo moiety will increase if (1) the weakest donor ligand is *trans* to the oxo bridge (N_{Trans} in this case) and (2) the Fe−O−Fe bond is linear to maximize Fe_{3d}−O_{2p} π overlap. A wealth of crystallographic data on $[TPA(X)Fe-O-Fe(X)TPA]^{+n}$ complexes exist in the literature,[8,25] and the above predictions are observed for **1a**, **1c**, and **1d** which exhibit ∠Fe−O−Fe approaching 180° and the $\{N,N\}_{trans}$ TPA configuration.[8a,c,d] It is clear, however, that small structural changes can introduce alternative TPA geometries as **1b** and **1e** show mixed $\{N,PY\}_{trans}$ configurations[8b,e] while $\mathbf{1}_f$ is $\{PY,PY\}_{trans}$.[8f] Of particular note in this series is the complex **1b**, which has the smallest ∠Fe−O−Fe = 138.9°, caused by an intramolecular hydrogen bond between aqua and hydroxide ligands. Although less preferred from an electronic standpoint, the $\{N,PY\}_{trans}$ arrangement serves to alleviate the steric interaction between pyridine α-hydrogens from adjacent TPA ligands at smaller Fe−O−Fe angles.

The $\{N,PY\}_{trans}$ configuration persists for **1b** in acetonitrile solution according to UV−vis, ^{1}H NMR, and resonance Raman data.[8b,d] Electronic spectra are particularly sensitive to Fe−O−Fe angle[5c] and are therefore a good metric for TPA configuration: oxo-to-iron LMCT transitions at 550−700 nm blue-shift as the Fe−O−Fe angle increases while a d−d transition at 490−500 nm is relatively constant. The result is that linear complexes such as **1a** have relatively featureless UV−vis spectra as the LMCT band shifts underneath the d−d band while bent complexes such as **1b** have a distinct oxo-to-iron

dx.doi.org/10.1021/ic5014347 | Inorg. Chem. 2014, 53, 11507−11516

LMCT band above 600 nm. The visual manifestation of this phenomenon is that **1b** takes on a distinct green color while **1a** and **1c** are red/orange.

The concentration of **1b** is maximal at pH 4.8 (Figure 1), and yet a green color was never observed during pH titrations; the color of the solution remained orange over the pH range 5.6–2.1. Disruption of the intramolecular hydrogen bond in **1b** by intermolecular interactions in aqueous solution would not be unexpected, but in the absence of additional spectroscopic data the configuration of the TPA ligands in **1b** cannot be determined.

Iron(III)–TPA Reduction by Hydroquinone. Stabile diferric complexes are the resting state of enzymes such as Hr, RR, and sMMO, and reduction to the diferrous state is required before O_2 activation may occur.[4] Enzymatically this is accomplished with an oxidoreductase, but iron(III) dimers may also be reduced by a variety of chemical means.[9] The reaction of **1** with hydroquinone (HQ) was investigated, and it was found that 1 equiv of HQ quantitatively produced benzoquinone and 2 equiv of iron(II) (eq 8).[26] The ferrous product

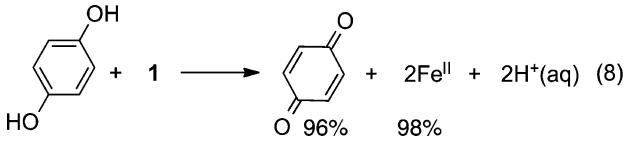

presumably exists as $[Fe(TPA)]^{+2}(aq)$, but the speciation was not determined. This reactivity is analogous to that of the binuclear type-3 copper enzymes catechol oxidase and tyrosinase, as well as many synthetic copper model systems.[6,27]

Reaction of **1** with 1,2-dihydroxybenzene (catechol) forms an iron(III) complex with a UV–vis spectrum consistent with $[Fe(TPA)(catecholate)]^+$ (data not shown).[11] This species is stable under anaerobic conditions; however, it reacts with O_2 to oxidatively cleave the catechol ring. This complex is a catechol dioxygenase model, and its reactivity is thought to be caused by admixture of an iron(II)–semiquinonate configuration in the iron(III) ground state.

Reaction Kinetics. Data on the reaction of **1** with hydroquinone at pH 5.6 are consistent with the following mechanism: Compounds **1a–c** are in rapid equilibrium with

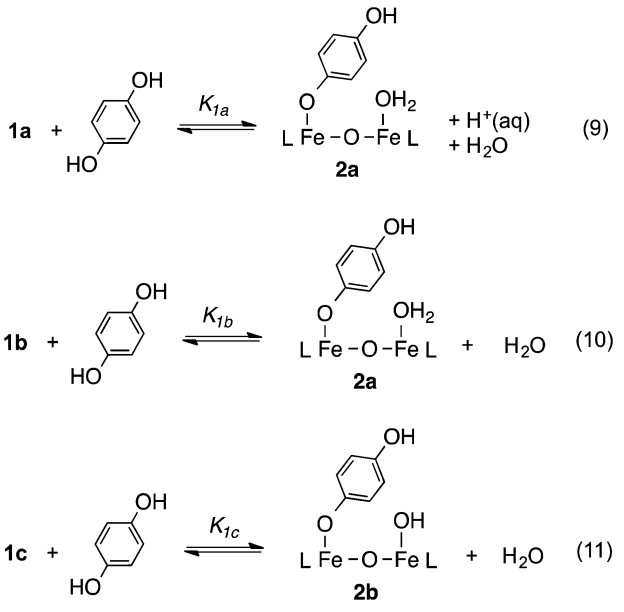

the iron(III)–hydroquinone adduct **2a,b** (eqs 9–11, L = TPA); note that only two protonation states of **2** are relevant because the coordinated phenol is completely ionized.[28] Intermediate **2** undergoes rate-determining inner-sphere electron transfer to release a semiquinone radical anion (SQ^-) from a mixed-valent $\{Fe^{II},Fe^{III}\}$ dimer (eq 12). This step is essentially irreversible as

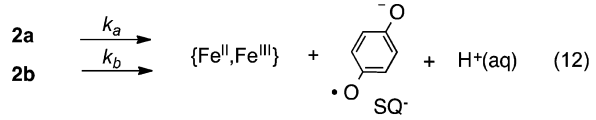

SQ^- will rapidly reduce another equivalent of iron(III) and produce benzoquinone in the observed 2:1 Fe:HQ stoichiometry (eq 13). Stable mixed-valent $Fe^{II}–O–Fe^{III}$ species are

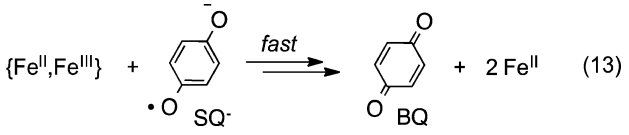

rare,[3] and the fate of the putative $\{Fe^{II},Fe^{III}\}$ intermediate would either be rapid reduction by semiquinone or decomposition to $[Fe^{II}(TPA)](aq)$ and half an equivalent of **1**. The protons released during the oxidation of HQ are buffered by excess TPA present in solution.

$$-\frac{1}{2}\frac{d[Fe_T^{III}]}{dt} = k_a[\mathbf{2a}] + k_b[\mathbf{2b}] = k'[\mathbf{2}] \quad (14)$$

$$k' = \alpha_{2a}k_a + \alpha_{2b}k_b \quad (15)$$

$$-\frac{d[Fe_T^{III}]}{dt} = \frac{k'K_{1c}\frac{\alpha_{1c}}{\alpha_{2b}}[HQ][Fe_T^{III}]}{1 + K_{1c}\frac{\alpha_{1c}}{\alpha_{2b}}[HQ]} = k_{obs}[Fe_T^{III}] \quad (16)$$

The rate of reaction is given by eq 14 where $[\mathbf{2}] = [\mathbf{2a}] + [\mathbf{2b}]$. The composite rate constant k' is a pH-weighted average of k_a and k_b where α_{2a} and α_{2b} are the mole fractions of **2** in protonation states a and b respectively (eq 15). The final rate law given in eq 16 is expressed in terms of the observable total iron(III) concentration (Fe_T^{III}) and is derived from eqs 9–11 and the Fe_T^{III} mass balance equation (see Supporting Information). The reaction was monitored by UV–vis as shown in Figure 2 where the band at 495 nm represents $[Fe_T^{III}]$.[29] With excess HQ the reaction is first order in Fe_T^{III} (Figure 2 inset, Figure S3 in the Supporting Information), and the rate constant k_{obs} was obtained from plots of A_{495} vs time. The dependence of k_{obs} on [HQ] was measured over the concentration range 30–80 mM[30] (60–160 equiv relative to Fe^{III}). Figure 3 shows a plot of k_{obs} vs [HQ]. Saturation kinetics are confirmed by fitting eq 16 to these data, and the parameters $K_{1c}(\alpha_{1c}/\alpha_{2b}) = 25(3)\ M^{-1}$ and $k' = 0.56(9)\ s^{-1}$ were obtained. Note that because $\alpha_{1c}/\alpha_{2b} \approx 1$ at pH 5.6 (see Supporting Information) 25 M^{-1} approximates the binding constant K_{1c}.

Intermediate **2** is formulated as an iron(III) phenoxide in which a H_2O/OH^- ligand on **1** has been replaced by hydroquinone. This is favored over a noncovalent **1**/HQ adduct based on the UV–vis spectra collected during the reaction: The intermediate species is distinctly different from **1** alone (bold spectrum in Figure 2) and is qualitatively similar to the stable **1**/phenol complex discussed below. If intermediate **2** is electronically similar to $[Fe(TPA)(catecholate)]^+$ and possesses significant iron(II)–semiquinonate character, SQ

dx.doi.org/10.1021/ic5014347 | Inorg. Chem. 2014, 53, 11507–11516

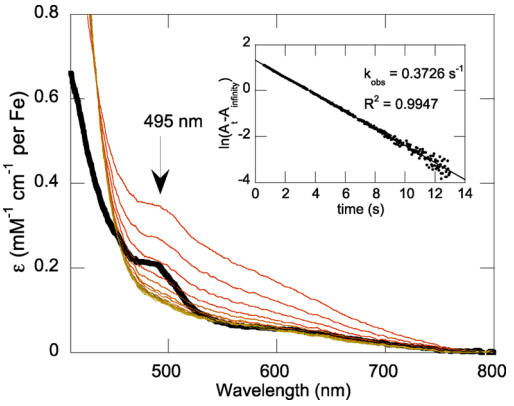

Figure 2. Absorption spectra taken during the reduction of **1** by hydroquinone at pH 5.56. Conditions: $[Fe^{3+}]_o$ = 0.99 mM; [TPA] = 10.0 mM; $[HQ]_o$ = 80.0 mM; 25 °C; I = 0.100 M; interval between spectra = 111 ms. Heavy black line: identical solution of **1** in the absence of HQ. Inset: Log plot of the integrated absorbance from 485 to 505 nm taken at 32 ms intervals shows first order kinetics.

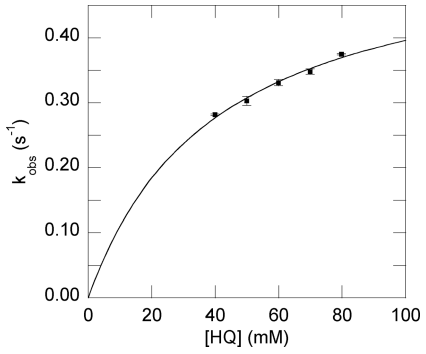

Figure 3. Observed first order rate constant vs [HQ] at pH 5.58(5); $[Fe^{3+}]_o$ = 0.99 mM; [TPA] = 10.0 mM; 25.0 ± 0.1 °C; I = 0.100 M; k_{obs} reported as the average of at least 4 separate experiments with error bars given as the standard deviation. Solid line: eq 16 fit to data; $K_{1c}(\alpha_{1c}/\alpha_{2b})$ = 25(3) M^{-1} and k' = 0.56(9) s^{-1}.

release from **2** (which does not occur with catechol) may be explained by the lack of chelate stabilization with hydroquinone.

Reduction of $M_2(\mu\text{-O})$ complexes generally increases the basicity of the oxo bridge,[31] so an additional driving force for the reaction is proton transfer to the μ-O ligand from solvent, i.e., eq 12 is formulated as proton-coupled electron transfer (PCET; either a concerted or stepwise mechanism).[32] A similar biochemical reaction involving iron(III) is the oxidation of unsaturated fatty acids by soybean lipoxogenase in which the Fe^{3+}–OH active site is reduced to Fe^{2+}–OH_2 by a PCET mechanism.[33] Reduction of synthetic diamond cores by PCET has also been observed in the manganese complexes $[L_2Mn^{IV}(\mu\text{-O})_2Mn^{III}L_2]^{+3}$ and $[L_2Mn^{III}(\mu\text{-O})(\mu\text{-OH})Mn^{III}L_2]^{+3}$ (L = phen), which are reduced to $[L_2Mn^{III}(\mu\text{-OH})_2Mn^{II}L_2]^{+3}$ by hydrogen atom donors such as 9,10-dihydroanthracene.[34]

Perhaps the most similar example to the title system is the reduction of the diiron(III) complex $[Fe_2(\mu\text{-O})(OH)_2(phen)_4]^{+2}$ by hydroquinone where a mechanism analogous to eqs 9–13 has been proposed.[9a] Saturation kinetics were not found from UV–vis experiments because observation of the intensely colored $[Fe(phen)_3]^{+2}$ product necessitated lower $[Fe_T^{III}]$ than in the TPA system, but the authors' second order rate constant of 15 M^{-1} s^{-1} is comparable to **1**: at low [HQ] eq 16 becomes second order with an apparent rate constant $k'K_{1c}(\alpha_{1c}/\alpha_{2b})$ = 14 M^{-1} s^{-1}. Although the equilibrium constant for HQ binding to $[Fe_2(\mu\text{-O})(OH)_2(phen)_4]^{+2}$ could not be evaluated, the authors estimated an upper limit of 100 M^{-1}, which is of the same order of magnitude as the binding constant K_{1c}. For additional comparison, an equilibrium constant of 8.9 M^{-1} has been measured for the binding of urea to **1b**.[5a]

The importance of proton transfer in the rate-limiting step was assessed with a proton inventory experiment in which the observed first order rate constant k_L was measured as a function of n, the deuterium mole fraction in the reaction medium (Figure 4). The linear relationship between k_L and n suggests

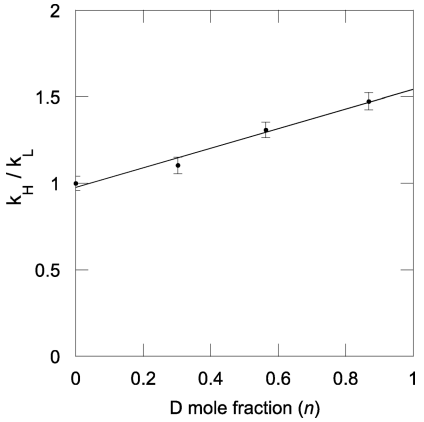

Figure 4. Proton inventory for the reaction of **1** with hydroquinone in mixed H/D media at pL = 5.56 (L = H, D). Conditions: $[Fe^{3+}]_o$ = 0.98 mM; [TPA] = 9.8 mM; $[HQ]_o$ = 59.9 mM; 25 °C. k_H/k_D = 1.5 from extrapolation to n = 1.

transfer of a single proton in the rate-limiting step.[35a] Extrapolation to n = 1 gives a modest kinetic isotope effect k_H/k_D = 1.5. Isotope effects in PCET may span several orders of magnitude;[35b] however, this example is similar to another iron(III) complex in which reduction of the metal is also coupled to ligand protonation. The isotope effect k_H/k_D = 2.3 was measured for degenerate PCET to $[Fe^{III}(Hbim)(H_2bim)_2]^{+2}$ (H_2bim = 2,2′-bi-imidazoline), in which iron(III) reduction is coupled to proton transfer to a distal bi-imidazoline N atom.[36]

pH-Dependent Speciation of Iron(III)–Phenoxides. In an attempt to probe the relative reactivity of complexes **1a–c**, the oxidation of HQ was investigated at varying pH. It was expected that the increase in positive charge on the oxidant by protonation of hydroxide ligands would increase the rate of reaction, but the opposite trend was observed. At lower pH the rate of reaction slowed and was no longer first order in $[Fe_T^{III}]$. The slope of log plots of A_{495} vs time data developed a distinct curvature in the pH range 4.1–5.2 (Figure S3 in the Supporting Information), indicating a change in reaction mechanism as compared with pH 5.6. The spectral profile of the reaction also changed: a new iron(III) band at 611 nm was observed that decayed during the course of the reaction (Figure 5). The final iron(II) spectrum is approximately the same as at pH 5.6.

The spectra observed at pH 4.1 are consistent with a mononuclear iron(III)–phenoxide complex[37] formed by acidic cleavage of the μ-oxo dimer (eq 17). This reaction manifold has been rigorously demonstrated for the iron(III)–TPA derivative

dx.doi.org/10.1021/ic5014347 | Inorg. Chem. 2014, 53, 11507–11516

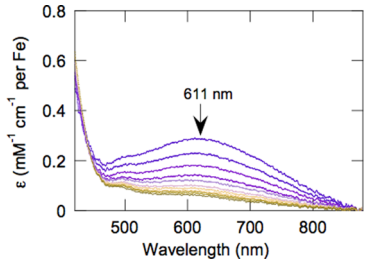

Figure 5. Reaction of **1** with hydroquinone at pH 4.14. Conditions: $[Fe^{3+}]_o$ = 0.91 mM; [TPA] = 9.2 mM; $[HQ]_o$ = 60.1 mM; 25 °C; I = 0.100 M; interval between spectra = 40 ms.

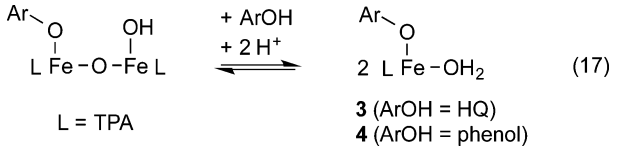

5 (Chart 2), which is an intramolecular version of the title system in which the phenoxy ligand is covalently bound to a

Chart 2. Mononuclear Iron(III)–TPA Phenoxide Complex Analogous to Intermediate 3[a]

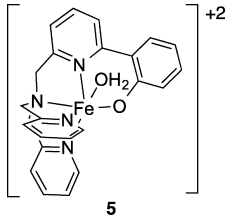

[a]See ref 38.

pyridyl α carbon.[38] Mass spectral, crystallographic, and resonance Raman data are consistent with an equilibrium process for **5** analogous to eq 17 that is shifted in either direction by addition of triethylamine or $HClO_4$. Mononuclear complex **5** is violet in color with a phenoxide-to-iron LMCT band at 600 nm; μ-oxo dimer formation causes a shift in this band to 486 nm and a corresponding color change to orange.

The hypothesis that μ-oxo dimer cleavage was occurring during the reaction of **1** with HQ was investigated using phenol, a redox-inactive proxy for hydroquinone.[39] A spectrophotometric titration of **1** with phenol in aqueous solution is shown in Figure 6. At circumneutral pH the solution had a red-orange color due to a band at 471 nm. The intensity reached a maximum at pH 6.4. Addition of HNO_3 decreased the intensity of the band at 471 nm, until a new band appeared at 570 nm as the pH approached 4. Visually the color of the solution changed to dark purple. The high and low pH limits in Figure 6 are also similar to the UV–vis spectra observed for the reaction of **1** with hydroquinone at pH 5.6 and 4.1 respectively (Figures 2 and 5). The spectral profile of the aqueous titration in Figure 6 is very similar to the titration reported for **5** in acetonitrile. To help confirm that the same process (eq 17) is occurring in both systems, a titration of iron(III)–TPA phenoxide complexes with triethylamine in acetonitrile was also performed. The results are shown in Figure S6 in the Supporting Information and are nearly identical to the aqueous titration in Figure 6. This supports the conclusion that iron(III)–TPA phenoxide complexes exist in a monomer–dimer equilibrium in both aqueous and organic solvents, whether the phenoxide is covalently bound to the TPA ligand (i.e., **5**) or is an independent ligand (i.e., **3** or **4**).

Further investigation of the coordination chemistry of **1** with phenol in aqueous solution was limited by the solubility of the iron(III)–phenoxide complexes: [phenol] > 110 mM caused precipitation of a dark oily product at the upper end of the pH range, and $NaNO_3$ added to control ionic strength salted the complex out of solution.[40] This precluded stability constant determination for this system. At lower pH, the mononuclear complex remained soluble and increasing the phenol concentration resulted in an increase in intensity of the band at 570 nm. This observation along with a lack of isosbestic points during the titration leads to the conclusion that iron(III) is not fully complexed by phenol and that other species besides those found in eq 17 must also be present. The molar absorptivities of the phenoxide complexes are substantially larger than those of **1a–c**,[41] such that the presence of the latter would be obscured in Figure 6.

The assignment of the purple species formed at low pH as a mononuclear iron(III)–TPA phenoxide complex is supported by a crystal structure of $[Fe(TPA)(2\text{-naphtholate})(OCH_3)]ClO_4$ (**6**). Addition of triethylamine to iron(III)–TPA and 2-naphthol in methanol produced a dark purple solution from which single crystals suitable for X-ray diffraction grew upon standing. The solid-state structure of **6** is shown in Figure 7 with select structural parameters given in Table 2. The electronic absorption spectrum of **6** redissolved in dichloromethane has a band at 540 nm (ε = 1800 M^{-1} cm^{-1}; see Figure S7 in the Supporting Information) which is analogous to the spectra of the other mononuclear iron(III)–TPA phenoxides discussed previously (**3**, **4**, and **5**). The Cambridge Structural Database contains no entries for iron(III)–TPA complexes

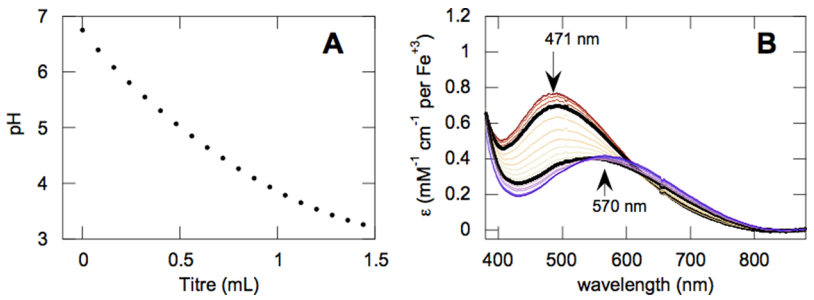

Figure 6. Spectrophotometric titration of **1**/phenol from pH 6.76 to 3.26. Conditions: $[Fe^{3+}]$ = 1.01 mM; [TPA] = 1.50 mM; [phenol] = 110 mM; 25.0 ± 0.1 °C; titrant = 0.1 M HNO_3. (A) pH titration curve. (B) Absorption spectra at each point during the titration; as the pH is lowered, the band at 471 nm decreases while the band at 570 nm increases. Bold spectra: pH 5.6 and 4.1 for comparison with Figures 2 and 5.

dx.doi.org/10.1021/ic5014347 | Inorg. Chem. 2014, 53, 11507–11516

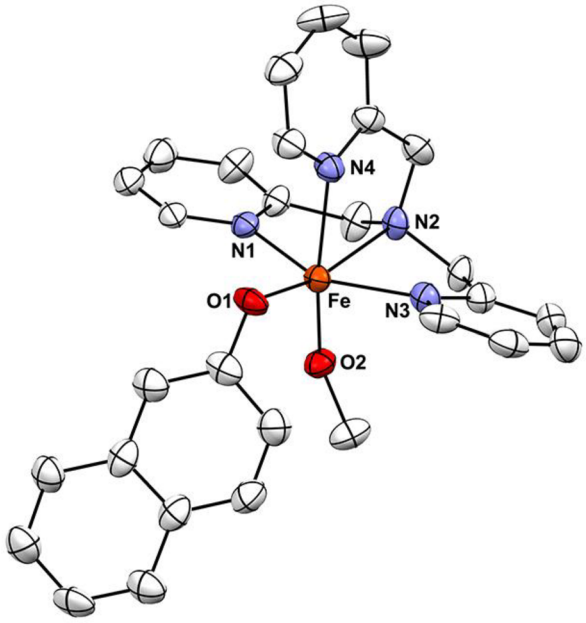

Figure 7. Displacement ellipsoid plot (50% probability level) of one of the two crystallographically independent $[Fe(TPA)(2\text{-naphtholate})(OCH_3)]^+$ cations at 110(2) K. The H atoms were omitted for the sake of clarity. **6**: FW = 619.85 amu, long dark red lath, 0.51 × 0.07 × 0.03 mm^3, monoclinic, $P2_1$ (no. 4), a = 13.2646(2), b = 15.2234(3), c = 13.7942(3) Å, β = 90.4308(15)°, V = 2785.42(9) $Å^3$, Z = 4, D_x = 1.478 g cm^{-3}, μ = 5.655 mm^{-1}, T_{min}–T_{max} 0.262–0.848. 24135 reflections were measured up to a resolution of $(\sin\theta/\lambda)_{max}$ = 0.62 $Å^{-1}$. 9907 reflections were unique (R_{int} = 0.0521), of which 9216 were observed [$I > 2\sigma(I)$]. 924 parameters were refined using 962 restraints. R1/wR2 [$I > 2\sigma(I)$]: 0.0599/0.1604. R1/wR2 [all reflections]: 0.06470.1669. S = 1.037. Residual electron density found between −0.49 and 1.00 e $Å^{-3}$.

Table 2. Selected Bond Lengths and Angles for $[Fe(TPA)(2\text{-naphtholate})(OCH_3)]ClO_4$

Bond Lengths (Å)			
Fe–N1	2.143(5)	Fe–N4	2.195(6)
	2.155(5)		2.205(5)
Fe–N2	2.251(4)	Fe–O1	1.896(4)
	2.220(5)		1.905(4)
Fe–N3	2.148(6)	Fe–O2	1.833(5)
	2.176(5)		1.838(5)
Bond Angles (deg)			
N1–Fe–N2	76.80(19)	O1–Fe–N2	165.5(2)
	75.6(2)		164.5(2)
N2–Fe–N3	74.80(19)	O2–Fe–N4	166.7(2)
	76.7(2)		166.92(19)
N2–Fe–N4	76.5(2)	O1–Fe–O2	104.2(2)
	77.49(19)		104.35(19)

with monodentate aryloxide ligands; however, **6** is structurally similar to several complexes bearing chelating phenoxides, notably $[Fe(TPA)(catecholate)]BPh_4$ (**7**) and $[Fe(TPA)(salicylate)]OTf$ (**8**, OTf = triflate).[11a,42] All three complexes are distorted octahedra exhibiting similar N–Fe–N compression caused by the chelating TPA ligand (average N_{PY}–Fe–N_{alkyl} angles are 76.3(0.9)° for **6**, 78(2)° for **7**, and 78(2)° for **8**). All three complexes have the aryloxide ligand *trans* to the N_{alkyl} TPA donor (although this is required by symmetry for **7**) with similar Fe–OAr distances of 1.896(4) and 1.905(4) Å for **6**, 1.90(1) and 1.90(1) Å for **7**, and 1.859(3) Å for **8**.

Formation of mononuclear iron(III) phenoxides substantially complicates the rate law for the reaction of **1** with HQ. The order in $[Fe_T^{III}]$ becomes fractional, and a second term for the reaction of intermediate **3** must be included. Because eq 17 consumes protons, there must be an upper pH limit at which **3** may be neglected and the rate law reverts to eq 16. The bold spectrum in Figure 6 indicates that the **1**/phenol system is approaching the μ-oxo dimer limit at pH 5.6. Assuming this is also true for **1**/hydroquinone, Michaelis Menten type saturation kinetics are expected at this pH. A complete derivation of the rate law and justification for its conversion to eq 16 at pH 5.6 are given in the Supporting Information.

CONCLUSIONS

The chelating ligand tris(pyridylmethyl)amine controls Fe^{3+}(aq) hydrolysis by stabilizing the $[Fe–O–Fe]^{+4}$ unit and preventing polymerization and precipitation of FeOOH(s). Aqueous Fe^{3+}/TPA mixtures self-assemble into (TPA)(X)Fe-(μ-O)Fe(X)(TPA) where, in the absence of better donor ligands, X is derived from solvent. Complex **1a** (X = H_2O) is a diprotic acid, and $pK_{a1,2}$ were determined to be 4.38(14) and 5.26(9). At pH < 3, protonation and hydration of the oxo bridge forms mononuclear $[Fe(TPA)]^{+3}$(aq). The aqueous speciation of this system is consistent with data from previous studies of iron(III)–TPA complexes in the solid state and acetonitrile solution.

Phenols readily displace the solvent occupying the labile coordination sites in **1**. Addition of phenol to **1** produces a new species with a strong chromophore attributed to phenoxide-to-iron(III) LMCT. The speciation is pH-dependent: a red-orange μ-oxo dimer (λ_{max} = 471 nm) is found at circumneutral pH while a purple mononuclear iron(III)–phenoxide (λ_{max} = 570 nm) begins to dominate as the pH approaches 4. When compound **1** is treated with the readily oxidizable phenol hydroquinone, quantitative conversion to iron(II) and benzoquinone is observed. At pH 5.6, saturation kinetics are consistent with equilibrium formation of a μ-oxo–diiron(III)–hydroquinone adduct (**2**) followed by rate-limiting electron transfer to iron. Intermediate **2** is spectroscopically similar to **4**, the analogous phenol complex of **1**. The equilibrium constant for formation of the μ-oxo diiron(III) hydroquinone complex (i.e., K_M^{-1}) is 25(3) M^{-1}, and the rate constant for its irreversible decomposition is 0.56(9) s^{-1}. A proton inventory experiment in mixed H/D media at pL = 5.56 shows a linear relationship between the observed first order rate constant and the deuterium mole fraction (n). Extrapolation to n = 1 gives the kinetic isotope effect k_H/k_D = 1.5. In the pH range 4.1–5.2 reduction of **1** by excess hydroquinone is no longer first order. This is attributed to conversion of the intermediate diiron(III)–hydroquinone adduct to the mononuclear complex **3**. The pH-dependent equilibrium between mono- and dimeric iron(III)–TPA aryloxide complexes is supported by spectrophotometric titration experiments on a redox-stable phenol derivative in both acetonitrile and water, and from a crystal structure of the monomeric iron(III) complex $[Fe(TPA)(2\text{-naphtholate})(OCH_3)]ClO_4$ (**6**).

ASSOCIATED CONTENT

Supporting Information

Summary of refined stability constants, tabulated pK_a values for iron(III)–aquo complexes, kinetic data from the reaction of **1**

dx.doi.org/10.1021/ic5014347 | Inorg. Chem. 2014, 53, 11507–11516

with hydroquinone, complete derivation of the proposed rate law, absorption spectra of iron(III)−TPA phenoxide complexes in acetonitrile, molar absorptivity of compound **6** in CH_2Cl_2, and crystallographic information file (CIF) for compound **6**. This material is available free of charge via the Internet at http://pubs.acs.org.

AUTHOR INFORMATION

Corresponding Author

*E-mail: will.kerber@bucknell.edu.

Notes

The authors declare no competing financial interest.

ACKNOWLEDGMENTS

We are grateful for financial support provided by Bucknell University, the Swanson endowment for new faculty in science and engineering, and the donors of the American Chemical Society Petroleum Research Fund (50877-UNI3). W.D.K. thanks Jack Raup for designing and building cables for spectrophotometer TTL triggering.

REFERENCES

(1) Flynn, C. M. *Chem. Rev.* **1984**, *84*, 31−41.

(2) (a) Tipping, E. *Cation Binding by Humic Substances*; Cambridge Environmental Chemistry Series; Cambridge University Press: Cambridge, 2002.

(3) Kurtz, D. M. *Chem. Rev.* **1990**, *90*, 585−606.

(4) (a) Friedle, S.; Reisner, E.; Lippard, S. J. *Chem. Soc. Rev.* **2010**, *39*, 2768−2779. (b) Tshuva, E. Y.; Lippard, S. J. *Chem. Rev.* **2004**, *104*, 987−1012. (c) Wallar, B. J.; Lipscomb, J. D. *Chem. Rev.* **1996**, *96*, 2625−2658.

(5) The bridging ligand X includes carboxylates/dicarboxylates, phosphate/phosphinates, carbonate, urea, sulfate, molybdate and vanadate. (a) Kryatov, S. V.; Rybak-Akimova, E. V.; Nazarenko, A. Y.; Robinson, P. D. *Chem. Commun.* **2000**, *11*, 921−922. (b) Holz, R. C.; Elgren, T. E.; Pearce, L. L.; Zhang, J. H.; O'Connor, C. J.; Que, L., Jr. *Inorg. Chem.* **1993**, *32*, 5844−5850. (c) Norman, R. E.; Holz, R. C.; Menage, S.; O'Connor, C. J.; Zhang, J. H.; Que, L., Jr. *Inorg. Chem.* **1990**, *29*, 4629−4637. (d) Norman, R. E.; Yan, S.; Que, L.; Backes, G.; Ling, J.; Sanders-Loehr, J.; Zhang, J. H.; O'Connor, C. J. *J. Am. Chem. Soc.* **1990**, *112*, 1554−1562.

(6) Que, L.; Tolman, W. B. *Angew. Chem., Int. Ed.* **2002**, *41*, 1114−1137.

(7) (a) Do, L. H.; Xue, G.; Que, L., Jr.; Lippard, S. J. *Inorg. Chem.* **2012**, *51*, 2393−2402. (b) Xue, G.; Pokutsa, A.; Que, L., Jr. *J. Am. Chem. Soc.* **2011**, *133*, 16657−16667. (c) Johansson, A. J.; Noack, H.; Siegbahn, P. E. M.; Xue, G.; Que, L., Jr. *Dalton Trans.* **2009**, *34*, 6741−6750. (d) Martinho, M.; Xue, G.; Fiedler, A. T.; Que, L., Jr.; Bominaar, E. L.; Münck, E. *J. Am. Chem. Soc.* **2009**, *131*, 5823−5830. (e) Xue, G.; Fiedler, A. T.; Martinho, M.; Münck, E.; Que, L. *Proc. Natl. Acad. Sci. U.S.A.* **2008**, *105*, 20615−20620. (f) Xue, G.; Wang, D.; De Hont, R.; Fiedler, A. T.; Shan, X.; Münck, E.; Que, L. *Proc. Natl. Acad. Sci. U.S.A.* **2007**, *104*, 20713−20718. (g) Zheng, H.; Zang, Y.; Dong, Y.; Young, V. G.; Que, L. *J. Am. Chem. Soc.* **1999**, *121*, 2226−2235. (h) Hsu, H.-F.; Dong, Y.; Shu, L.; Young, V. G.; Que, L. *J. Am. Chem. Soc.* **1999**, *121*, 5230−5237. (i) Zang, Y.; Dong, Y.; Que, L., Jr.; Kauffmann, K.; Münck, E. *J. Am. Chem. Soc.* **1995**, *117*, 1169−1170.

(8) **1a**: (a) Whittlesey, B. R.; Pang, Z.; Holwerda, R. A. *Inorg. Chim. Acta* **1999**, *284*, 124−126. **1b**: (b) Hazell, A.; Jensen, K. B.; McKenzie, C. J.; Toftlund, H. *Inorg. Chem.* **1994**, *33*, 3127−3134. **1c**: (c) Min, K. S.; Rhinegold, A. L.; Miller, J. S. *J. Am. Chem. Soc.* **2006**, *128*, 40−41. **1d**: (d) Wilkinson, E. C.; Dong, Y.; Que, L., Jr. *J. Am. Chem. Soc.* **1994**, *116*, 8394−8395. **1e**: (e) Min, K. S.; Arif, A. M.; Miller, J. S. *Inorg. Chim. Acta* **2007**, *360*, 1854−1858. **1f**: (f) Kojima, T.; Leising, R. A.; Yan, S.; Que, L., Jr. *J. Am. Chem. Soc.* **1993**, *115*, 11328−11335.

(9) (a) Bhattacharyya, J.; Mukhopadhyay, S. *Trans. Met. Chem.* **2006**, *31*, 256−261. (b) Bhattacharyya, J.; Das, S.; Mukhopadhyay, S. *Dalton Trans.* **2007**, 1214−1220. (c) Mukherjee, R.; Dhar, B. B.; Banerjee, R. *Polyhedron* **2006**, *25*, 1367−1372. (d) Zang, Y.; Pan, G.; Que, L., Jr.; Fox, B. G.; Münck, E. *J. Am. Chem. Soc.* **1994**, *116*, 3653−3654. (e) Bhattacharyya, J.; Dutta, K.; Mukhopadhyay, S. *Dalton Trans.* **2004**, *18*, 2910−2917. (f) Mukherjee, R.; Bijayi Dhar, B.; Banerjee, R.; Mukhopadhyay, S. *J. Coord. Chem.* **2006**, *59*, 1157−1165. (g) Mandal, P. C.; Bhattacharyya, J.; Das, S.; Mukhopadhyay, S.; Kirschenbaum, L. J. *Polyhedron* **2009**, *28*, 3162−3168. (h) Bhattacharyya, J.; Mukhopadhyay, S. *Helv. Chim. Acta* **2005**, *88*, 2661−2674.

(10) Que, L., Jr. *Coord. Chem. Rev.* **1983**, *50*, 73−108.

(11) (a) Simaan, A. J.; Boillot, M.-L.; Carrasco, R.; Cano, J.; Girerd, J.-J.; Mattioli, T. A.; Ensling, J. R.; Spiering, H.; Gutlich, P. *Chem.—Eur. J.* **2005**, *11*, 1779−1793. (b) Jang, H. G.; Cox, D. D.; Que, L., Jr. *J. Am. Chem. Soc.* **1991**, *113*, 9200−9204.

(12) Basett, J.; Denney, R. C.; Jerrery, G. H.; Mendham, J. *Vogel's Textbook of Quantitative Inorganic Analysis*; Longman Group: Essex, U.K., 1986.

(13) (a) Gans, P.; O'Sullivan, B. *Talanta* **2000**, *51*, 33−37. (b) GLEE, Protonic Software, 2000; http://www.hyperquad.co.uk/glee.htm (accessed June 16, 2014).

(14) VLpH, Protonic Software, 2005; http://www.hyperquad.co.uk/vlph.htm (accessed June 16, 2014).

(15) (a) Gans, P.; Sabatini, A.; Vacca, A. *Talanta* **1996**, *43*, 1739−1753. (b) Hyperquad2008, Protonic Software, 2008; http://www.hyperquad.co.uk/HQ2008.htm (accessed June 16, 2014).

(16) (a) Byrne, R. H.; Yao, W.; Luo, Y.; Wang, B. *Mar. Chem.* **2005**, *97*, 34−48. (b) Djurdjević, P.; Stankov, M. J.; Odović, J. *Polyhedron* **2000**, *19*, 1085−1096.

(17) (a) Alderighi, L.; Gans, P.; Ienco, A.; Peters, D.; Sabatini, A.; Vacca, A. *Coord. Chem. Rev.* **1999**, *184*, 311−318. (b) Hyperquad Simulation and Speciation (HySS2009), Protonic Software, 2009; http://www.hyperquad.co.uk/hyss.htm (Accessed June 16, 2014).

(18) Salomaa, P.; Schaleger, L. L.; Long, F. A. *J. Am. Chem. Soc.* **1964**, *86*, 1−7.

(19) Leighton, P. A.; Forbes, G. S. *J. Am. Chem. Soc.* **1929**, *51*, 3549−3559.

(20) (a) Wolsey, W. C. *J. Chem. Educ.* **1973**, *50*, A335. (b) Raymond, K. N. *Chem. Eng. News* **1983**, *61* (49), 4−5.

(21) (a) Bergh, A.; Offenhartz, P.; George, P.; Haight, G. *J. Chem. Soc.* **1964**, 1533−1538. (b) Mukherjee, G. N.; Das, A. *Proc. Indian Acad. Sci.* **2002**, *114*, 163−174. (c) Costa, J.; Delgado, R.; Drew, M. G. B.; Félix, V. *J. Chem. Soc., Dalton Trans.* **1999**, *24*, 4331−4339.

(22) The exact value is not well-agreed upon due to complications associated with hydrolysis and precipitation, see: Perrin, D. D. *Ionisation constants of inorganic acids and bases in aqueous solution*, 2nd ed.; Pergamon Press: Oxford, U.K.; 1982; pp 62−64.

(23) Another species rejected from the model is the cyclic trimer $[Fe(\mu\text{-}O)(TPA)]_3^{+3}$. Although known in the solid state, this structure is less plausible in solution, and titration data could not be successfully refined when it was included. See: Kryatov, S. V.; Taktak, S.; Korendovych, I. V.; Rybak-Akimova, E. V.; Kaizer, J.; Torelli, S.; Shan, X.; Mandal, S.; MacMurdo, V. L.; Mairata i Payeras, A.; Que, L. *Inorg. Chem.* **2005**, *44*, 85−99.

(24) (a) Longhinotti, E.; Domingos, J. B.; Szpoganicz, B.; Neves, A.; Nome, F. *Inorg. Chim. Acta* **2005**, *358*, 2089−2092. (b) Neves, A.; Terenzi, H.; Horner, R.; Horn, A., Jr.; Szpoganicz, B.; Sugai, J. *Inorg. Chem. Commun.* **2001**, *4*, 388−391.

(25) A variety of complexes in which the *cis* sites are occupied by an additional bridging ligands have also been characterized; see ref 5.

(26) Yields were determined at pH 4. At pH 5.6 quantitative formation of iron(II) was still observed, but BQ gradually decomposed, so an accurate yield could not be determined; see ref 19.

(27) Mayer, A. M. *Phytochemistry* **2006**, *67*, 2318−2331.

(28) (a) Desai, A. G.; Milburn, R. M. *J. Am. Chem. Soc.* **1969**, *91*, 1958−1961. (b) McBryde, W. *Can. J. Chem.* **1968**, *46*, 2385−2392.

(29) A_{495} is proportional to $[Fe_T^{III}]$ because all of the iron-containing species present at pH 5.6 have an appreciable absorbance at 495 nm

(**1a**−**c**, **2a**,**b**, and Fe^{II}(TPA)) while none of the organic species do (TPA, HQ, BQ, SQ^{-}).
(30) Hydroquinone concentration was limited by solubility. The most concentrated HQ solutions used in this work (160 mM which gives 80 mM HQ after 1:1 mixing with iron(III)−TPA) were approaching the solubility limit when $NaNO_3$ was added to control ionic strength.
(31) Baldwin, M. J.; Pecoraro, V. L. *J. Am. Chem. Soc.* **1996**, *118*, 11325−11326.
(32) (a) Hammes-Schiffer, S.; Stuchebrukhov, A. A. *Chem. Rev.* **2010**, *110*, 6939−6960. (b) Mayer, J. M. *Acc. Chem. Res.* **2011**, *44*, 36−46.
(33) (a) Hammes-Schiffer, S. *Acc. Chem. Res.* **2006**, *39*, 93−100. (b) Fukuzumi, S. *Helv. Chim. Acta* **2006**, *89*, 2425−2440.
(34) Larsen, A. S.; Wang, K.; Lockwood, M. A.; Rice, G. L.; Won, T.-J.; Lovell, S.; Sadílek, M.; Tureček, F.; Mayer, J. M. *J. Am. Chem. Soc.* **2002**, *124*, 10112−10123.
(35) (a) Quinn, D. M. Theory and Practice of Solvent Isotope Effects. In *Isotope Effects in Chemistry and Biology*; Kohen, A., Limbach, H. H., Eds.; CRC Press: Boca Raton, FL, 2006; pp 995−1018. (b) Hammes-Schiffer, S. Kinetic Isotope Effects for Proton-Coupled Electron Transfer Reactions. In *Isotope Effects in Chemistry and Biology*; Kohen, A., Limbach, H. H., Eds.; CRC Press: Boca Raton, FL, 2006; pp 499−519.
(36) Roth, J. P.; Lovell, S.; Mayer, J. M. *J. Am. Chem. Soc.* **2000**, *122*, 5486−5498.
(37) (a) Lever, A. B. P. *Inorganic Electronic Spectroscopy*, 2nd ed.; Elsevier: New York, 1984; pp 310−320. (b) Wesp, E. F.; Brode, W. R. *J. Am. Chem. Soc.* **1934**, *56*, 1037−1042. (c) Kunkely, H.; Vogler, A. *Inorg. Chem. Commun.* **2003**, *6*, 1335−1337.
(38) Jensen, M. P.; Lange, S. J.; Mehn, M. P.; Que, E. L.; Que, L. *J. Am. Chem. Soc.* **2003**, *125*, 2113−2128.
(39) No iron(II) was measured by the 1,10-phenanthroline method from mixtures of **1** and phenol. Stable iron(III)−phenoxide complexes were also observed with 4-methylphenol, 4-bromophenol, 4-nitrophenol, and 2-naphthol. In each case UV−vis spectra similar to Figure 6 are observed, but all attempts to crystallize derivatives of **2** for structural characterization have failed.
(40) Precipitation was never observed during the reaction of **1** with HQ; evidently the additional hydrophilic OH group on hydroquinone is enough to maintain aqueous solubility.
(41) At pH 5.6 the effective molar absorptivity at 471 nm of the phenoxide complex (Figure 6) is 0.677 mM^{-1} cm^{-1} per Fe^{3+} while a spectrophotometric titration of **1** alone (data not shown) gives an effective molar absorptivity of 0.119 mM^{-1} cm^{-1} per Fe^{3+} at this wavelength. At pH 4.1, a molar absorptivity comparison at 570 nm gives 0.394 and 0.027 mM^{-1} cm^{-1} per Fe^{3+} for the phenoxide complex and **1** respectively.
(42) Makhlynets, O. V.; Das, P.; Taktak, S.; Flook, M.; Mas-Balleste, R. N.; Rybak-Akimova, E. V.; Que, L., Jr. *Chem.—Eur. J.* **2009**, *15*, 13171−13180.